PROCEEDINGS OF SCIENCE

Performance of the Horizontally Polarized Antennas Used in the Radio Neutrino Observatory in Greenland

Bryan Hendricks[a,*] **for the RNO-G Collaboration**
(a complete list of authors can be found at the end of the proceedings)

[a] *Dept. of Physics, Penn State University, University Park, PA 16802, USA*
E-mail: blh5615@psu.edu

Radio detection of ultra-high energy neutrinos via the Askaryan effect has enabled a new generation of immense, cost-effective neutrino detectors due to the long attenuation lengths of radio signals in dense dielectric media. The Radio Neutrino Observatory in Greenland (RNO-G) is one such detector with a unique view of the northern hemisphere; it is being built at the top of Greenland's ice cap to take advantage of the low noise environment and large detection volume available in the pure ice. It currently has 7 fully operational independent autonomous stations spaced roughly 1 km apart and once completed will comprise 35 stations. Each station contains both a shallow component with broadband, high-gain antennas and an in-ice component with three strings of broadband, omnidirectional horizontally and vertically polarized antennas. Both polarization modes are needed to reconstruct the arrival direction of detected neutrinos. Here we discuss the design, simulation, validation, production, deployment, and performance of RNO-G's horizontally polarized antennas.

The 38th International Cosmic Ray Conference (ICRC2023)
26 July – 3 August, 2023
Nagoya, Japan

*Speaker

PoS(ICRC2023)1133

1. Introduction

While ultra-high energy cosmic rays (UHECRs) have been observed for decades, their sources have not been unambiguously determined. As charged particles, their paths en route to Earth are misdirected due to the magnetic fields between their source and the Earth. UHECRs are expected to create UHE neutrinos (E > 10 PeV) by interacting in their source environment and on their journey to Earth via their interaction with the cosmic microwave background. Since neutrinos are neutral, nearly massless subatomic particles that primarily interact through the weak force, their paths are not deflected. This means they point back to their source. However, due to their low interaction cross sections, immense detector volumes are needed to reach the sensitivities necessary given their expected fluxes at UHEs.

The complications of needing massive detector volumes can be alleviated by using Askaryan radio emission from UHE neutrino interactions in dense dielectric media. Radio waves have long attenuation lengths, so enormous detectors can be built with sparsely populated independent stations. This makes radio detectors especially suitable for near-future UHE neutrino discovery [1]. One such detector is the Radio Neutrino Observatory in Greenland (RNO-G) which is being built at the peak of Greenland's ice cap. It will have 35 independent stations spaced roughly 1 km apart to maximize the effective volume of the detector, for a radio attenuation length which has been measured to exceed 700 m [2] at the site.

RNO-G intercepts the incident radio emission with antennas of three primary types: log-periodic dipole antennas (LPDAs) for the shallow component, vertically polarized (Vpol) antennas for the trigger and reconstruction, and horizontally polarized (Hpol) antennas primarily for direction reconstruction. The Hpol and Vpol antennas are deployed in three 100 m deep, 28.5 cm diameter boreholes per station. The linear polarization of Askaryan radiation allows us to pinpoint where on the Cherenkov emission cone a detection occurred so long as we are able to measure both the vertical and horizontal polarization of the signal [3]. This location information is crucial for fully reconstructing the signal and neutrino arrival direction, but developing an antenna for the horizontal polarization is challenging due to the physical constraint of the borehole diameter. In this contribution, we will present the design process used to remedy some of these difficulties for RNO-G's Hpol antennas, their performance, and their production and deployment.

2. Hpol Antenna Performance Goals

The Askaryan signal expected from UHE neutrinos is highly impulsive in the time-domain, leading to a broadband radio signal in the Fourier domain. The passband of RNO-G's signal chain is 130 - 700 MHz to capture this broadband signal [2]. Since Askaryan emission is the result of coherent Cherenkov emission (coherence condition met when $\lambda \gg$ shower width) [4], it is strongest at the Cherenkov angle. In ice, that angle is roughly 56°. Off-cone, however, coherence is lost. This accelerates at higher frequencies as the wavelength decreases relative to the shower width [5]. Additionally, the effective length of the antennas naturally falls with increasing frequency [6]. The lower frequencies of RNO-G's passband are thus of higher priority when designing the antenna. Designing an antenna that is sensitive to the lower end of this frequency range is very difficult in the horizontal polarization as the borehole has a diameter of 28.5 cm, yet antennas typically resonate

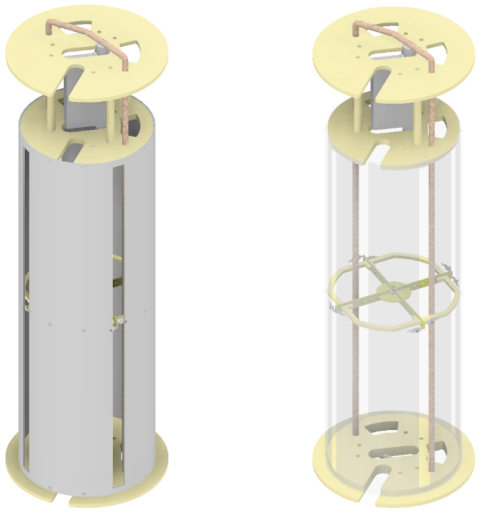

Figure 1: Left: Hpol antenna with the tube hidden to reveal the inner structure. Right: Full Hpol antenna. In addition to the antenna itself, nylon end caps and deployment rope can be seen in the figures as well as the low-noise amplifier (LNA) between the top two end caps.

when their physical dimensions are on the order of the wavelength of the impinging signal, and the wavelength corresponding to 130 MHz in air is 2.3 m.

While the lower frequencies are prioritized, it is important to be able to detect signals in as much of the frequency range of interest as possible. However, developing a geometry-constrained antenna in this broad of a range is difficult, as it must be impedance matched to its 50 Ω receiver to reduce signal reflection and maximize the signal-to-noise ratio. Since the antennas have both inductive and capacitive reactance, which are both a function of frequency, the broader the frequency range the harder it is to match, especially by tuning geometric parameters alone. As a result, a matching circuit is necessary.

As the neutrino flux at the location of the antenna is expected to have azimuthal symmetry, the antenna should have a corresponding gain pattern.

3. Antenna Parameters and Design

Our Hpol antenna design (see Fig. 1) attempts to mitigate the challenge of resonating at low frequencies in a borehole constricted space by taking advantage of Booker's antenna modification of Babinet's principle [7] which states that a slot in a flat conducting plane (known as a slot antenna) will have a radiation pattern that mimics a dipole of the same dimensions but with its E-field and B-field interchanged. This results in a vertical slot having a horizontal E-field polarization, and the primary difference aside from the field swap is that the impedance is modified by a constant factor. Similar to a dipole, resonance can occur when the slot is on the order of $\lambda/2$. Given our 130 - 700 MHz passband and shipping and deployment constraints on the length, 60 cm was chosen for the slot length.

A simple slot antenna on a flat sheet suffers from a null in the azimuthal direction aligned with the plane of the sheet, which does not meet our azimuthal symmetry requirement. To alleviate this asymmetry, the sheet is essentially wrapped into a cylinder (see vertical openings in Fig. 1). In

practice, this is done by milling a cylindrical aluminum tube. This allows the antenna to interact with the B-field via the changing magnetic flux through the cylinder, which can be thought of as many stacked loops. This eliminates the null in the azimuthal direction, and if the cylinder's diameter is small compared to the wavelength, this provides good azimuthal symmetry. However, the diameter is also tied to the bandwidth.

The bandwidth of a dipole antenna can be increased by widening the dipole. The same is accomplished in our case by increasing the diameter of the cylinder. This comes with a trade-off in azimuthal symmetry [8]. To obtain both azimuthal symmetry and high bandwidth, we make up for the larger diameter by adding additional slots to the cylinder. Four slots and an eight inch (20.32 cm) diameter proved to be an effective compromise between antenna performance, ease of production, cost, weight, and borehole constraints. To ensure the increased range of signals received by the widened antenna are minimally reflected (caused by impedance mismatch across the band), we developed a matching circuit using a tuned combination of surface-mount capacitors and inductors on the centerfeed arms between each antenna slot terminals and the receiving feed (see green, central object in Fig. 1).

The gain of the Hpol antennas is primarily dictated by the diameter of the cylinder, which has already been set to eight inches as described above to enable deployment with minimal issues. While the gain is primarily controlled by the antenna geometry, it does not give the full picture for one's ability to extract a signal from an antenna. The Hpol signal is read out using a 50 Ω impedance port that feeds into the rest of the signal chain. Any mismatch in impedance between the antenna and the feed (and then throughout the rest of the signal chain) results in a portion of the incident signal being reflected, which leads to standing waves within the transmission line and reduced signal strength as a result. The extent of this mismatch is commonly characterized by a quantity called the S_{11}, which in dB is given by:

$$S_{11} = 10 \log_{10} \left(\frac{P_{ref}}{P_{inc}} \right) \tag{1}$$

The gain of an antenna is then reduced accordingly, and the result called the realized gain:

$$G_{realized} = G_{absolute}(1 - |S_{11}|^2) \tag{2}$$

where the magnitude of the S_{11} is in linear units. This can also be calculated from a similar quantity called the voltage standing wave ratio, or VSWR, which represents the ratio between the incident and the standing wave voltage amplitude resulting from reflections and is reported in linear units and calculated from the S_{11} as:

$$VSWR = \frac{1 + |S_{11}|}{1 - |S_{11}|} \tag{3}$$

Measurements and simulation of these parameters for RNO-G's Hpol antennas are presented in the following section.

4. Measurements and Simulation

VSWR measurements of every Hpol antenna used in RNO-G's first (2021) and second (2022) deployment season were taken and compared against XFdtd (Remcom's 3D electromagnetic simu-

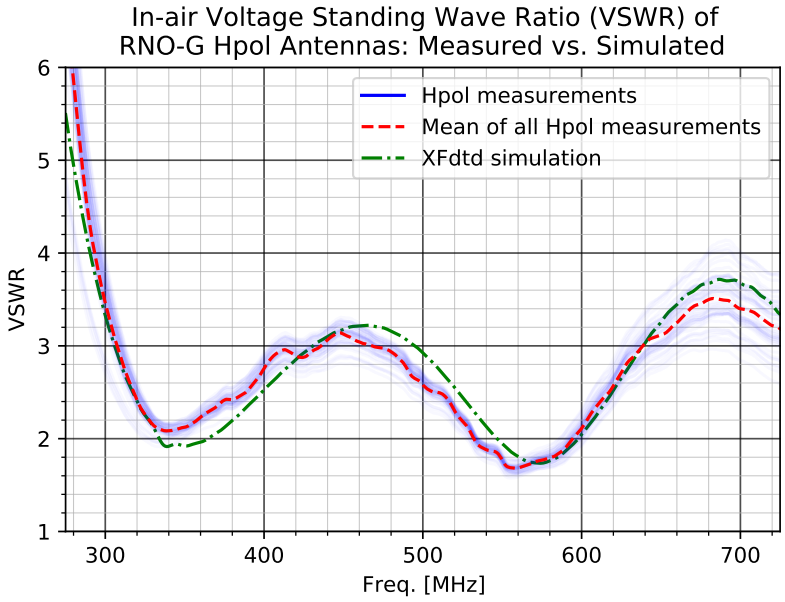

Figure 2: VSWR measurements of all Hpol antennas shipped for RNO-G's first deployment season and XFdtd simulation for comparison.

lation software that uses the finite-difference time-domain method) simulation to validate the latter and give an estimate of the systematics (see Fig. 2). Due to practical difficulties in replicating the in-ice environment, each measurement, and therefore the simulation for comparison, was done in air. The maximum root mean square error (RMSE) between the simulation and all measured antennas is 13.8% within the antenna's bandwidth. We define the Hpol antenna bandwidth as the region where the mean antenna measurement falls below 3.5 VSWR within the signal chain's 130-700 MHz passband, which is 300-700 MHz. Additionally, there is a maximum $1\sigma/mean$ variance of only 10.0% between all of the Hpol antenna measurements.

A similar comparison of the azimuthal (boresight) gain was done for a single Hpol antenna measured in an anechoic chamber vs. simulation between 450 and 750 MHz (see Fig. 3), limited by the transmitter's frequency range, normalized to 0 dB. All frequencies can be seen to be azimuthally symmetric within ±1.77 dB, on the same order of symmetry as the simulation. The discontinuity in the measured values is due to the nature of the measurement setup requiring the full azimuthal sweep to be done in two halves, obtaining the 180° - 360° portion of the pattern by returning the mount to the original location and manually rotating the antenna by 180° before resuming the sweep. There was no precise way to do this manual rotation at the time, so the small but non-zero displacement from the original position as well as the potential offset from a perfect 180° rotation produces the discontinuity. Forthcoming absolute measurements, rather than just relative as reported here, will be performed all the way down to 300 MHz with a mount capable of precise rotation to improve our knowledge of the systematics. These measurements will also include increments in zenith.

In addition to VSWR and gain systematics, there is additional uncertainty introduced by potential offsets of the Hpol antennas in the borehole. While practical considerations currently prevent us from doing this study in the field, an in-ice simulation was developed from the in-

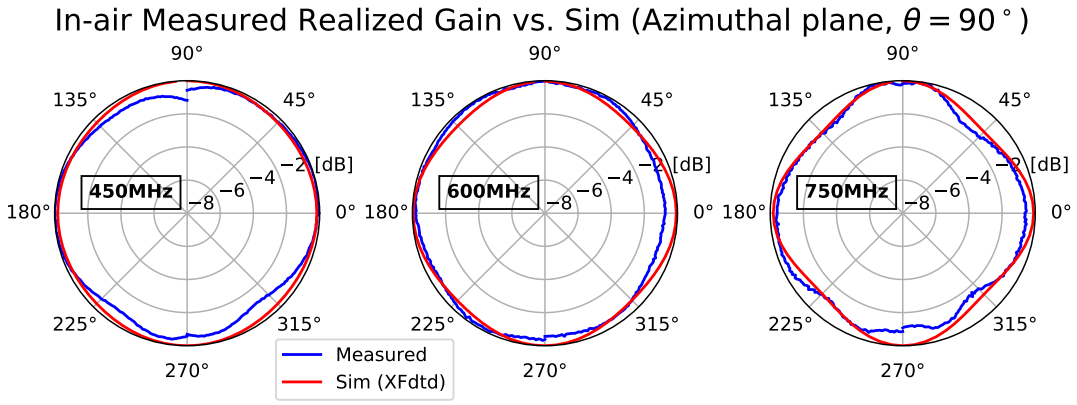

Figure 3: Realized gain measurements taken in an anechoic chamber in the azimuthal plane (boresight zenith angle) of an Hpol antenna at four frequencies and simulation for comparison, all normalized to 0 dB.

air simulation with the addition of a block of ice with a borehole. As the Hpol antenna moves closer/further from the ice, it couples more/less in that direction. Since we do not have a way of measuring this offset for our deployed antennas, this contributes to our systematics. To limit the offset while still allowing relative ease of deployment, end caps (see top nylon portion of Fig. 1), primarily in place to house electronics such as the low-noise amplifier and power/signal cables and allow the antennas to be tied in to the deployment string, were designed to extend beyond the outer diameter of the antennas. The Hpol antenna end caps are 24 cm in diameter, so with the 28.5 cm diameter borehole this limits the offset to just 2.25 cm in any direction.

Simulations were run at multiple offsets between 0 and 2.25 cm and the resulting response variations can be see in Fig. 4 in the form of the effective length (l_{eff}). The l_{eff} of an antenna represents its ability to convert incident EM radiation into a voltage signal and is calculated accordingly as:

$$V^{oc} = E^{i} \cdot l_{eff} \tag{4}$$

where V^{oc} represents the open-circuit voltage across the antenna's terminals and E^i the incident electric field strength. The solid lines for each color represent the ϕ component (the one that matters for Hpol antennas) of the l_{eff} at a given zenith angle. 0° zenith corresponds to directly above the Hpol antenna in the direction of the null, and 90° zenith corresponds to the boresight (maximum gain) angle. The shaded regions for each color represent the maximum deviations from the perfectly centered l_{eff} - for reference, the boresight deviation is 10.6% RMSE. The Hpol antenna systematics are summarized in Table 1.

Using an in-air version of the Hpol antenna simulation model shown in this contribution (its frequency response shifted to account for the change in index of refraction as detailed in [3]), it has been shown that the space angle resolution can reach the order of 10°. In a forthcoming study, the space angle resolution will be re-evaluated with the in-ice simulation and systematics shown here taken into account.

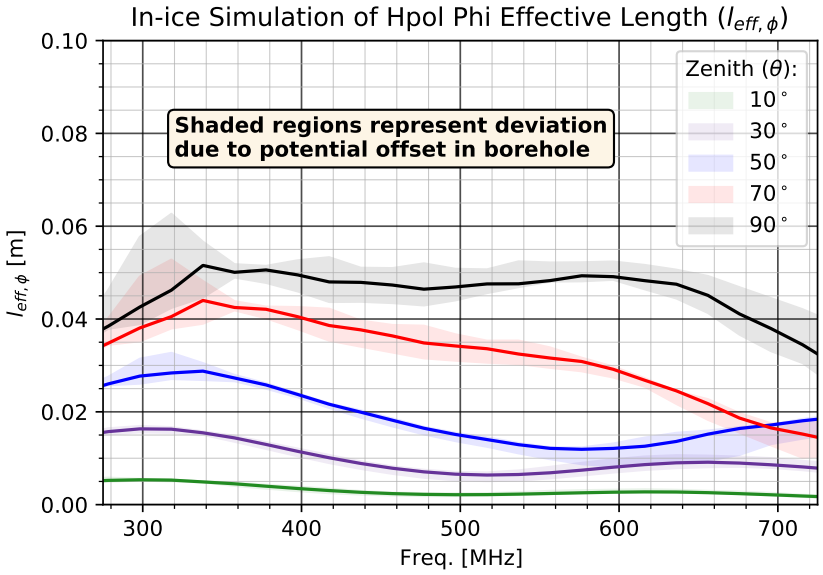

Figure 4: Hpol antenna phi effective length from 130 - 700 MHz at various zenith (inclination) angles with shaded regions representing the maximum deviation from the borehole center for all azimuths.

Systematics Summary				
Type	Measured	Measured	Sim to measured	Sim
Quantity	Azimuthal Gain	VSWR	VSWR	$l_{\text{eff, boresight}}$
Value	±1.77 dB	10.0% $\frac{1\sigma}{\text{mean}}$ variance	13.8% RMSE	10.6% RMSE

Table 1: A basic summary of currently understood Hpol antenna systematics including the voltage standing wave ratio, gain, and effective length. Each systematic is evaluated across the 300 - 700 MHz bandwidth of the antenna shown either through measurement and/or simulation.

5. Production and Deployment

At the writing of this article, RNO-G has deployed 7 of 35 stations over two drilling seasons with an additional 10 planned for the 2023 boreal summer season (see Fig. 5 left). Each antenna, including the nylon support pieces, can be aseembled from the individual components within about an hour. The weight of a fully assembled Hpol antenna is only 3.95 kg. Over 60 Hpol antennas have been built so far (see Fig. 5 right) and nearly 30 already deployed without issues. An additional 75 Hpol antennas are on track to be produced by the end of summer 2023, enabled by a streamlined production process amenable to mass production.

6. Conclusion

Creating Hpol antennas for deep, in-ice radio UHE neutrino detectors is challenging due to borehole size constraints from drilling limitations. RNO-G's Hpol antennas were designed to circumvent this limitation by taking advantage of Babinet's principle via slotted conductors which interact more strongly with fields perpendicular to their longest dimension, and to employ loops which interact with the vertical B-fields of the incident Hpol radio waves. This was realized as a 60

Figure 5: Left: Deploying a string of antennas into one of the many boreholes of RNO-G. Right: 60 Hpol antennas produced during RNO-G's first production season.

cm long cylindrical quad-slot aluminum tube with an impedance matching circuit. The antennas are robust, easy to mass produce, and have high simulation and antenna-to-antenna fidelity, lending themselves well to their use in current and future in-ice radio neutrino detectors. A future study will be done to evaluate the influence of Hpol antennas on direction reconstruction resolution with the most up-to-date in-ice simulation and systematics shown in these proceedings (including gain systematic updates mentioned in section 4).

References

[1] V. B. Valera, M. Bustamante, and C. Glaser *Phys. Rev. D* **107** (Feb, 2023) 043019.

[2] **RNO-G** Collaboration, J. A. Aguilar *et al.* *Journal of Glaciology* **68** no. 272, (May, 2022) 1234–1242.

[3] I. Plaisier, S. Bouma, and A. Nelles *The European Physical Journal C* **83** no. 5, (May, 2023) .

[4] G. Askaryan *J. Phys. Soc. Japan* **17** no. Suppl A, (1962) .

[5] **RNO-G** Collaboration, J. A. Aguilar *et al.* *JINST* **16** no. 03, (2021) P03025. [Erratum: JINST 18, E03001 (2023)].

[6] C. Glaser, A. Nelles, I. Plaisier, C. Welling, S. W. Barwick, D. García-Fernández, G. Gaswint, R. Lahmann, and C. Persichilli *The European Physical Journal C* **79** no. 6, (Jun, 2019) .

[7] H. Booker *Journal of the Institution of Electrical Engineers - Part IIIA: Radiolocation* **93** no. 4, (1946) 620–626.

[8] G. Sinclair *Proceedings of the IRE* **36** no. 12, (1948) 1487–1492.

Full Author List: RNO-G Collaboration

J. A. Aguilar[1], P. Allison[2], D. Besson[3], A. Bishop[10], O. Botner[4], S. Bouma[5], S. Buitink[6], W. Castiglioni[8], M. Cataldo[5], B. A. Clark[7], A. Coleman[4], K. Couberly[3], P. Dasgupta[1], S. de Kockere[9], K. D. de Vries[9], C. Deaconu[8], M. A. DuVernois[10], A. Eimer[5], C. Glaser[4], T. Glüsenkamp[4], A. Hallgren[4], S. Hallmann[11], J. C. Hanson[12], B. Hendricks[14], J. Henrichs[11,5], N. Heyer[4], C. Hornhuber[3], K. Hughes[8], T. Karg[11], A. Karle[10], J. L. Kelley[10], M. Korntheuer[1], M. Kowalski[11,15], I. Kravchenko[16], R. Krebs[14], R. Lahmann[5], P. Lehmann[5], U. Latif[9], P. Laub[5], C.-H. Liu[16], J. Mammo[16], M. J. Marsee[17], Z. S. Meyers[11,5], M. Mikhailova[3], K. Michaels[8], K. Mulrey[13], M. Muzio[14], A. Nelles[11,5], A. Novikov[19], A. Nozdrina[3], E. Oberla[8], B. Oeyen[18], I. Plaisier[5,11], N. Punsuebsay[19], L. Pyras[11,5], D. Ryckbosch[18], F. Schlüter[1], O. Scholten[9,20], D. Seckel[19], M. F. H. Seikh[3], D. Smith[8], J. Stoffels[9], D. Southall[8], K. Terveer[5], S. Toscano[1], D. Tosi[10], D. J. Van Den Broeck[9,6], N. van Eijndhoven[9], A. G. Vieregg[8], J. Z. Vischer[5], C. Welling[8], D. R. Williams[17], S. Wissel[14], R. Young[3], A. Zink[5]

[1] Université Libre de Bruxelles, Science Faculty CP230, B-1050 Brussels, Belgium
[2] Dept. of Physics, Center for Cosmology and AstroParticle Physics, Ohio State University, Columbus, OH 43210, USA
[3] University of Kansas, Dept. of Physics and Astronomy, Lawrence, KS 66045, USA
[4] Uppsala University, Dept. of Physics and Astronomy, Uppsala, SE-752 37, Sweden
[5] Erlangen Center for Astroparticle Physics (ECAP), Friedrich-Alexander-Universität Erlangen-Nürnberg, 91058 Erlangen, Germany
[6] Vrije Universiteit Brussel, Astrophysical Institute, Pleinlaan 2, 1050 Brussels, Belgium
[7] Department of Physics, University of Maryland, College Park, MD 20742, USA
[8] Dept. of Physics, Enrico Fermi Inst., Kavli Inst. for Cosmological Physics, University of Chicago, Chicago, IL 60637, USA
[9] Vrije Universiteit Brussel, Dienst ELEM, B-1050 Brussels, Belgium
[10] Wisconsin IceCube Particle Astrophysics Center (WIPAC) and Dept. of Physics, University of Wisconsin-Madison, Madison, WI 53703, USA
[11] Deutsches Elektronen-Synchrotron DESY, Platanenallee 6, 15738 Zeuthen, Germany
[12] Whittier College, Whittier, CA 90602, USA
[13] Dept. of Astrophysics/IMAPP, Radboud University, PO Box 9010, 6500 GL, The Netherlands
[14] Dept. of Physics, Dept. of Astronomy & Astrophysics, Penn State University, University Park, PA 16802, USA
[15] Institut für Physik, Humboldt-Universität zu Berlin, 12489 Berlin, Germany
[16] Dept. of Physics and Astronomy, Univ. of Nebraska-Lincoln, NE, 68588, USA
[17] Dept. of Physics and Astronomy, University of Alabama, Tuscaloosa, AL 35487, USA
[18] Ghent University, Dept. of Physics and Astronomy, B-9000 Gent, Belgium
[19] Dept. of Physics and Astronomy, University of Delaware, Newark, DE 19716, USA
[20] Kapteyn Institute, University of Groningen, Groningen, The Netherlands

Acknowledgments

We are thankful to the staff at Summit Station for supporting our deployment work in every way possible. We also acknowledge our colleagues from the British Antarctic Survey for embarking on the journey of building and operating the BigRAID drill for our project. We would like to acknowledge our home institutions and funding agencies for supporting the RNO-G work; in particular the Belgian Funds for Scientific Research (FRS-FNRS and FWO) and the FWO programme for International Research Infrastructure (IRI), the National Science Foundation (NSF Award IDs 2118315, 2112352, 211232, 2111410) and the IceCube EPSCoR Initiative (Award ID 2019597), the German research foundation (DFG, Grant NE 2031/2-1), the Helmholtz Association (Initiative and Networking Fund, W2/W3 Program), the University of Chicago Research Computing Center, and the European Research Council under the European Unions Horizon 2020 research and innovation programme (grant agreement No 805486).